Mechanism of Thermal Decomposition of Hydroxyacetone: A Flash Pyrolysis Vacuum Ultraviolet Photoionization Time-of-Flight Mass Spectrometry and Density Functional Theory Study

Xinghua Liu,[a] Ru Sun,[b] Kuanliang Shao,[c] Jingsong Zhang,[c,d,*]

[a] *School of Chemistry and Chemical Engineering, Hainan University, Haikou, Hainan 570228, PR China*
[b] *School of Food Science and Engineering, Hainan University, Haikou, Hainan 570228, PR China*
[c] *Department of Chemistry, University of California, Riverside, California 92521, United States*
[d] *Air Pollution Research Center, University of California, Riverside, California 92521, United States*

Abstract

Thermal decomposition mechanism of hydroxyacetone from 850 K to 1390 K was examined by using flash pyrolysis vacuum ultraviolet photoionization time-of-flight mass spectrometry (VUV-PI-TOFMS) combined with density functional theory (DFT) calculation. The results showed that keto-enol tautomerisms could occur prior to thermal decomposition of hydroxyacetone. The decomposition pathways of hydroxyacetone and its isomer 2-hydroxypropanal were characterized. The thermal decomposition reactions started at about 950 K. The homolysis reactions related to the cleavage of C_{CO}-C_{COH} bond of hydroxyacetone and 2-hydroxypropanal, as well as CH_3 loss of hydroxyacetone, dominated the initial decomposition reactions. The subsequent decompositions of the radical intermediates generated by the initial homolysis decompositions were the major secondary decomposition reactions. The formation pathways of small molecules, such as H_2, CH_4, H_2O and HCHO, were proposed to proceed via molecular elimination reactions facilitated by the active α-H atoms. These elimination reactions were not negligible at high temperatures above 1230

K.

Keywords: Bio-oil model compound, hydroxyacetone, thermal decomposition, mechanism.

* Corresponding author. Email: jingsong.zhang@ucr.edu; Tel +1 951 827 4197; Fax: +1 951 827 4713.

1. Introduction

Biomass, the largest renewable energy resource, is attracting more and more attention due to the depletion of fossil fuels, increasing energy demand, and environmental concerns.[1-2] Hydrogen and synthesis gas production via thermal and catalytic reforming techniques have been considered as one of the promising ways of biomass utilization.[3-6] Hydroxyacetone, also known as acetol, can be produced by pyrolysis of biomass-derived materials, such as cellulose,[7-9] hemicellulose,[10] sugar[11-12] and glycerol.[13-16] Hydroxyacetone is considered as the highest content in the ketone fraction and between the fifth and eighth of the major nonacidic compounds of bio-oil.[17-18] Therefore, the knowledge of the pyrolysis mechanism of hydroxyacetone is important for understanding the processes of steam reforming and thermal conversion of biomass/bio-oil. However, to date, only a few studies have been reported on this topic.

Ramos et al.[19] reported that H_2, CH_4, CO, CO_2 and C_2 species were produced in gaseous yields with the participation of steam via R1 in the non-catalytic process of hydroxyacetone over 450-650 °C. However, Bimbela et al.[17] suggested that steam did not participate in R1 in the steam

reforming of hydroxyacetone over 550-750 °C. Fuentes-Cano et al.[6] claimed that hydroxyacetone was thermally decomposed via R2 by stoichiometry.

$$CH_3COCH_2OH \xrightarrow{\text{Steam}} H_2 + CH_4 + CO + CO_2 + C_2 \text{ Species} \quad \text{R1}$$

$$CH_3COCH_2OH \longrightarrow H_2 + CH_4 + 2CO \quad \text{R2}$$

Wang et al.[20] proposed that the primary decomposition pathways of hydroxyacetone were methyl radical and hydrogen elimination via R3 and R4. Albuquerque et al.[21] pointed out that dehydrogenation of hydroxyacetone leads to pyruvaldehyde and H_2 through R5.

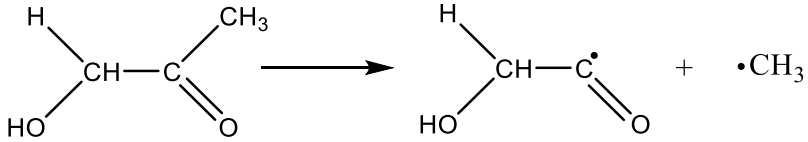

R3

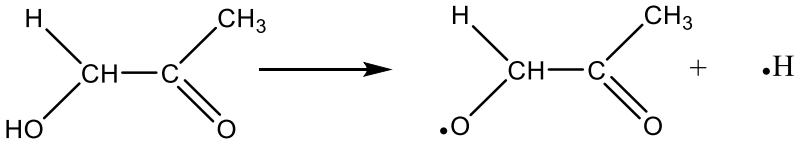

R4

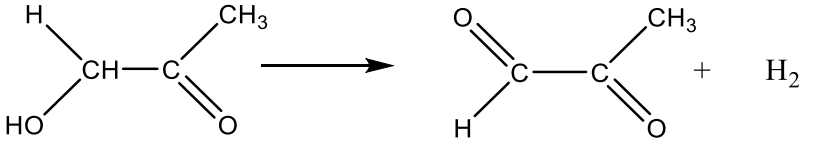

R5

Jing et al.[22] investigated the tautomerization and decomposition of hydroxyacetone using density functional theory (DFT) at the M06-2X/6-31G(2df,p) level. They found that the H atom could be eliminated via R6. This pathway also occurred in the catalytic oxidation process of hydroxyacetone.[23] In addition, the result showed that hydroxyacetone isomerized to 2-hydroxypropanal via H atom transfer with low barrier heights of about 40 kcal/mol. Then 2-hydroxypropanal decomposed via two competitive pathways to produce formaldehyde (R7) and methyl radical (R8), respectively.

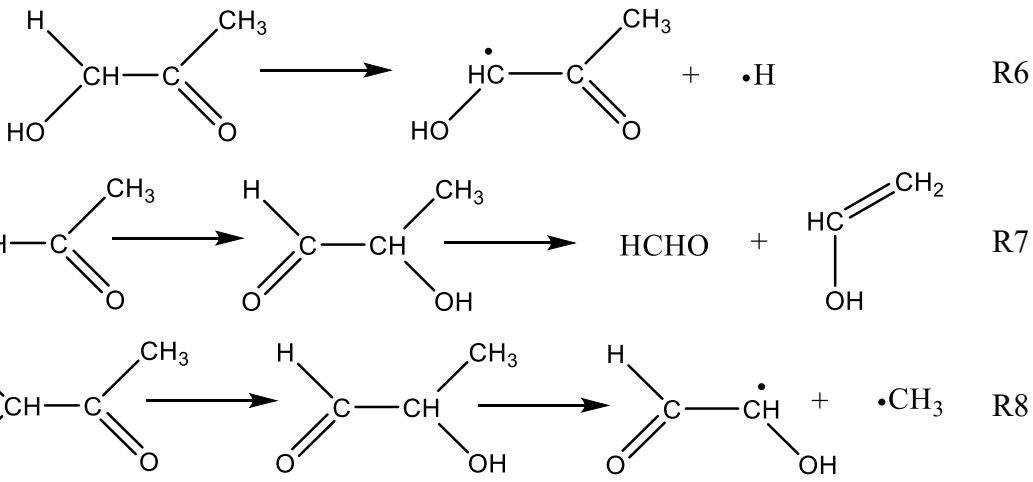

To the best of our knowledge, a thorough thermal decomposition mechanism of hydroxyacetone has not been reported. In this work, the mechanism was systematically investigated using a flash pyrolysis vacuum ultraviolet photoionization time-of-flight mass spectrometry (VUV-PI-TOFMS) combined with the DFT calculation. The experimental approach of flash pyrolysis coupled to supersonic expansion/molecular beam sampling and VUV-PI-TOFMS provides a short reaction time to investigate the initial steps of pyrolysis, supersonic cooling/molecular beam sampling to preserve the reaction intermediates and products, mass spectrometry detection of a broad range of reactive intermediates and products, and minimized ion fragmentation due to the low photoionization energy. The bond homolysis and molecular elimination pathways in the initial stage of pyrolysis can be directly observed simultaneously in this work, with minimal complication from the subsequent reactions. The detailed thermal decomposition mechanism of hydroxyacetone would benefit the understanding of thermal treatment of biomass and bio-oil.

2. Experimental and Computational Methods

The VUV-PI-TOFMS experimental setup has been described in detail previously.[24-28] Hydroxyacetone (Sigma Aldrich, 99%) was used in this work without further purification. The hydroxyacetone sample (~ 0.3%) was prepared by bubbling helium (~ 1.5 atm) through the hydroxyacetone liquid in a bubbler at room temperature.[29] The sample was transferred via a pulsed nozzle into a micro-pyrolyzer made of SiC tube (Carborundum, 40 mm long, heated length 10 mm, 2 mm O.D., 1 mm I.D.). The pyrolysis micro-reactor was based on the design described by Chen and co-workers.[30] The pyrolyzer was heated up to 1390 K by varying the electric current passing through the SiC tube. A type C thermocouple was attached to the pyrolyzer to measure the pyrolysis temperature. The gas flow properties in the SiC microreactor were investigated previously at elevated temperatures and at 1-2 atm backing pressure (i.e., under conditions similar to our experiment).[31-33] The speed of the sample flow was approximately sonic in the short, heated region, with a ~ 50 μs residence/reaction time for precursors in the He carrier gas. The very dilute concentration of the precursor in He buffer gas and short reaction time in the heated region favored unimolecular reactions, and bimolecular reactive collisions were estimated to be sufficiently minor except at very high temperatures (> 1400 K), as suggested by the modellings[32-33] and our previous study.[27] Similarly, under these experimental conditions, the intermediates produced from the initial thermal decompositions of the precursor would not undergo significant secondary decompositions at the initial and medium high temperatures (e.g., 900-1100 K) (due to the short reaction time and small decomposition rate constant of the precursor) until at more elevated temperatures. It should be noted that the distribution of pressure and temperature inside the microreactor was nonuniform

and likely not at equilibrium,[32-33] thus this work focused more on qualitative reaction mechanisms than quantitative kinetics. The gas pressure at the exit of the tube was still sufficient to produce a supersonic expansion and cooling; upon exiting from the heated reaction zone, the nascent products, intermediates, and any remaining reactants were sampled into and supersonically cooled in a molecular beam (with an internal temperature of 20-150 K),[30-31] which significantly reduced their internal energy and dissociative photoionization. Downstream in a high vacuum detection region, they were photoionized by a 118.2 nm (10.49 eV, 10 Hz) VUV radiation generated by tripling the 355 nm output of a Nd:YAG laser in a Xe gas cell (~ 20 Torr). The positively charged ions were extracted into a linear TOFMS and collected by a microchannel plate detector. The pyrolysis mass spectra were recorded in a digital storage oscilloscope. Each spectrum represented the averaged signal of 512 laser shots. The TOF spectra were then converted to the mass spectra.

DFT theory has been widely employed to investigate the pyrolysis mechanism of organic compounds.[12, 28, 34] In this work, the possible decomposition pathways were located at the (U)B3LYP/6-311++G(d,p) level of theory. Frequency and intrinsic reaction coordinate (IRC) calculations[35] were performed in order to ensure the accuracy of the transition states. Single point energies of related reactants, transition states, and products were calculated at the (U)B3LYP/6-311++G(d,p) level with zero point energy (ZPE) correction. The energy barrier was defined as the energy difference between the transition state and the corresponding reactant. All calculations were performed using the Gaussian 09 program.[36] The calculated single point energies at the (U)B3LYP/6-311++G(d,p) level are within 1.0 kcal/mol with respect to those of the CBS-QB3 method and within 2.0 kcal/mol with respect to those of UM06-2X/6-311++G(2df,2p) (see Table

S1 in Supporting Information (SI)), respectively, indicating a good accuracy of the (U)B3LYP/6-311++G(d,p) method. All the geometry coordinates of the species related to hydroxyacetone thermal decomposition are provided in SI.

Unimolecular reaction rate constants of the initiation reactions were calculated using transition state theory (TST). For the unimolecular dissociation reaction with a well-defined transition state, the rate constant was calculated using TST with Wigner tunneling correction.[37-40] The single point energy and frequencies of reactants and transition states were obtained from the DFT calculations at the (U)B3LYP/6-311++G(d,p) level of theory using the Gaussian 09 package as described before. For the bond homolysis (barrierless) reactions, variational transition state theory (VTST) with Wigner tunneling correction was applied.[37-40] A series of constrained optimizations along the reaction path were carried out, and at each optimized geometry ("trial transition state"), the potential energy and vibrational frequencies were calculated at the same level of theory. The dividing surfaces for the barrierless reactions at different temperatures were determined by finding the maximum Gibbs free energy change $\Delta G^{e}(T)$ of the "trial transition state" along the reaction pathway at individual temperatures. This computational protocol was similar to previous works,[41-43] All the rate constant calculations were performed using the KISTHELP program.[39, 44-45]

3. Results

3.1 Experiments of Thermal Decomposition of Hydroxyacetone

The mass spectra of hydroxyacetone pyrolysis over 295-1390 K are shown in Fig. 1 and 2. Two photoionization peaks at m/z 74 and 43 were found at 295 K. They corresponded to the hydroxyacetone parent mass peak and the CH_3CO^+ dissociative photoionization mass peak, respectively. Two other minor dissociative photoionization peaks at m/z 58 and 31 were also identified. The minor m/z 31 peak may be attributed to the ionization of $\cdot CH_2OH$, which is the coproduct of CH_3CO^+. The minor m/z 58 peak may be produced by CH_4 elimination via photoionization dissociation. As the pyrolysis temperature was increased, no new peaks were found in the range of 295-850 K. The first distinguishable peak produced by thermal decomposition was observed at m/z 45 at 950 K, and it grew significantly when the temperature increased from 950 K to 1140 K. It was the mass peak of the neutral C_2H_5O radical. It should be noted that the CH_3CO radical at m/z 43 could be formed by thermal decomposition of the parent molecule in this initial temperature range. The first sign of the appearance of the CH_3CO radical from thermal dissociation could not be determined clearly because it was mixed with the dissociative photoionization fragment peak of the parent at m/z 43. The production of the CH_3CO radical could be inferred indirectly because the intensity ratio of the m/z 43 peak and the parent peak increased slightly with the increasing temperature in this region. Methyl radical peak at m/z 15 was detected at 1140 K. It could be directly produced by unimolecular decomposition of hydroxyacetone. Another possible formation pathway of the methyl radical was subsequent decomposition of the CH_3CO radical, which could serve as additional evidence of the CH_3CO

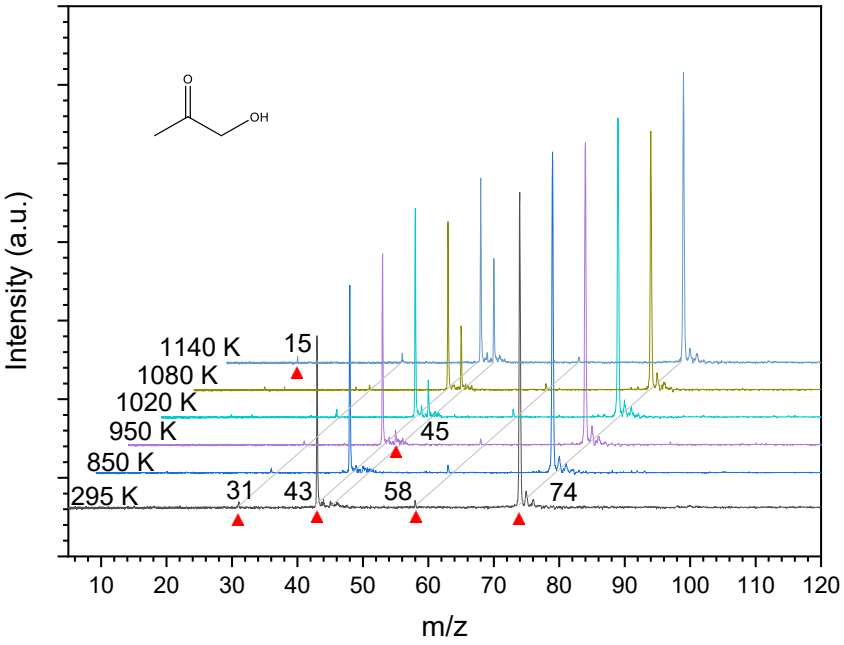

Fig. 1 Mass spectra of thermal decomposition of hydroxyacetone over 295-1140 K. The mass spectra are offset for clarity.

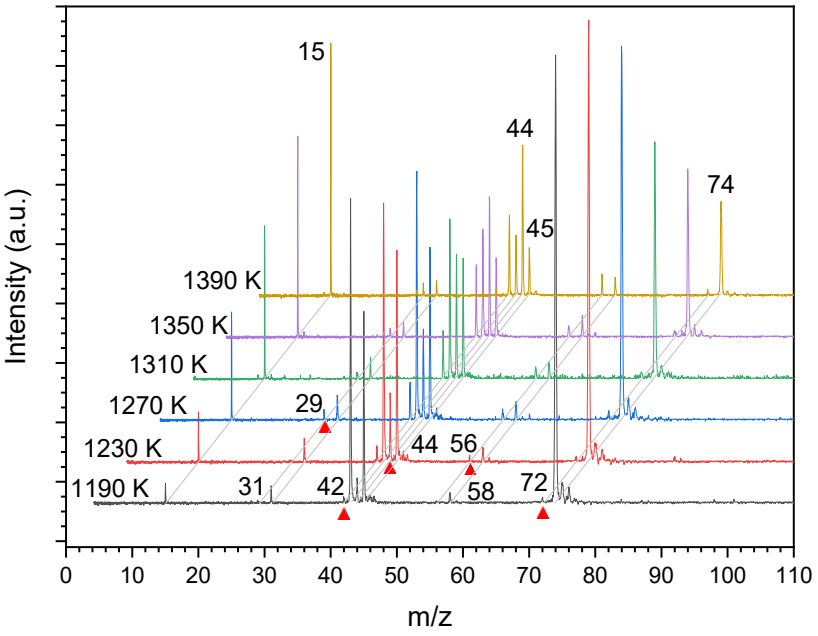

Fig. 2 Mass spectra of thermal decomposition of hydroxyacetone over 1190-1390 K. The mass spectra are offset for clarity.

radical production. Meanwhile, the intensity of the m/z 31 peak of the CH_2OH radical, the counterpart of the CH_3CO radical produced by C_{CO}-C_{COH} homolysis of hydroxyacetone, increased slightly. Therefore, it is reasonable to consider that the CH_3CO radical could be generated thermally at or above 1140 K.

The m/z 15 peak increased significantly from 1190 K to 1390 K. The m/z 31 peak increased modestly to its maximum intensity from 1190 K to 1270 K, then decreased slightly from 1310 K to 1390 K. Two small peaks at m/z 72 and 42 started to appear at 1190 K. The m/z 72 peak representing $C_3H_4O_2$ was probably formed by H_2 elimination of hydroxyacetone via R5. The m/z 72 peak remained a minor peak up to 1390 K. The m/z 42 peak was ketene ($H_2C=C=O$) formed by H loss of the CH_3CO radical. The m/z 42 peak increased significantly when the temperature increased from 1230 K to 1390 K. The peak at m/z 44 started to increase at 1190 K and became significant at and above 1230 K. The intensity ratio of the peak at m/z 43 to the peak at m/z 44 was about 4:1 at 1230 K, which was obviously larger than the ratio of the peak at m/z 43 to its ^{13}C isotopic peak at m/z 44. Therefore, the increased peak at m/z 44 above 1190 K may indicate the formation of ethenol by formaldehyde elimination of hydroxyacetone (rather than the isotopic effect of the peak at m/z 43). The formaldehyde counter fragment was not detected due to its high ionization energy (10.86 eV)[46] above the photon energy in this study. A small peak at m/z 56 corresponding to C_3H_4O was also found at 1230 K. It may be formed by H_2O elimination of hydroxyacetone or 2-hydroxypropanal (an isomer of hydroxyacetone and to be discussed in detail in the following section). The m/z 56 peak increased with increasing temperature up to 1390 K. The m/z 58 peak increased slightly from 1230 K to 1390 K. A small peak at m/z 59 appeared at

1230 K; this could be the co-fragment in the CH_3-loss channel of hydroxyacetone. A very minor peak at m/z 73 seems to appear at 1230 K, and it remained very small or barely present at higher temperatures. A peak at m/z 29 was observed at 1270 K. It might be the peak of the HCO radical. It was possibly formed as the counter fragment of $CH_3C(H)OH$ (m/z 45) from the C_{CO}-C_{COH} bond cleavage of $CH_3CH(OH)$-CHO (2-hydroxypropanal), which is an isomer of hydroxyacetone and will be discussed in detail in the following section. The m/z 45 peak ($CH_3C(H)OH$) increased to its maximum intensity at ~ 1250 K and then decreased at higher temperatures, indicating its secondary decomposition. An alternative source for the m/z 44 peak was H-atom loss of $CH_3C(H)OH$ forming ethenol or acetaldehyde. No new peaks of significant intensities were detected from 1310 up to 1390 K.

The intensities of the main peaks versus temperature are plotted in Fig. 3. The intensities of hydroxyacetone (m/z 74) and peak at m/z 43 decreased rapidly starting from 1190 K (as the main source of the m/z 43 peak was CH_3CO^+ from dissociative photoionization of the parent), while the intensities of the methyl radical (m/z 15), ketene (m/z 42) and ethenol (m/z 44) increased obviously starting from about the same temperature of ~ 1190 K. These indicate that the initial main stage of thermal decomposition of hydroxyacetone took place at and above 1190 K. The intensity of the C_2H_5O radical (m/z 45) gradually increased from 950 K and peaked at 1230 K, and then decreased with the increase of temperature, showing that the rate of the subsequent decomposition reactions of the C_2H_5O radical overcame the rate of its formation reactions. Besides the parent peak, the peak of the CH_3CO^+/CH_3CO radical at m/z 43 was prominent when the temperature was lower than 1310 K. The peak of the methyl radical became dominant at 1350 K and higher temperatures.

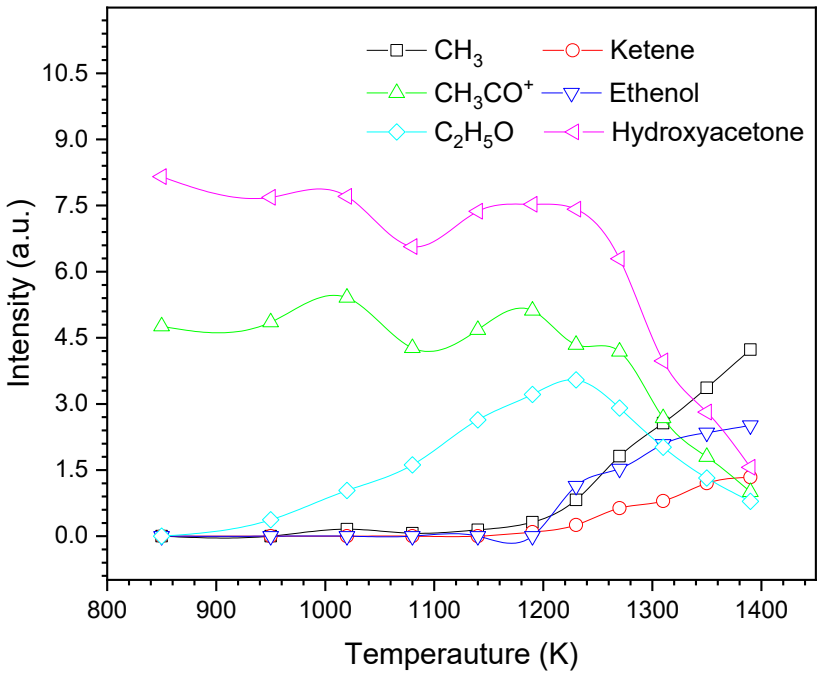

Fig. 3 Intensity evolution of the main peaks of hydroxyacetone pyrolysis over 850-1390 K.

3.2 Computational Results

3.2.1 Isomerization Reactions

The possible isomers and isomerization pathways of hydroxyacetone are shown in Scheme 1. Two stable conformers of hydroxyacetone are found. Syn-hydroxyacetone with intramolecular H-bond between the carbonyl group and hydroxyl group has a lower single point energy than anti-hydroxyacetone. The energy barrier between these two conformers is 5.1 kcal/mol. Keto-enol tautomerism is a typical isomerization of ketone. Different conformers lead to different tautomerism pathways. Syn-hydroxyacetone has three isomerization pathways corresponding to 3 different types of H migrating to the carbonyl group. The H in -CH_2- migrates to the carbonyl

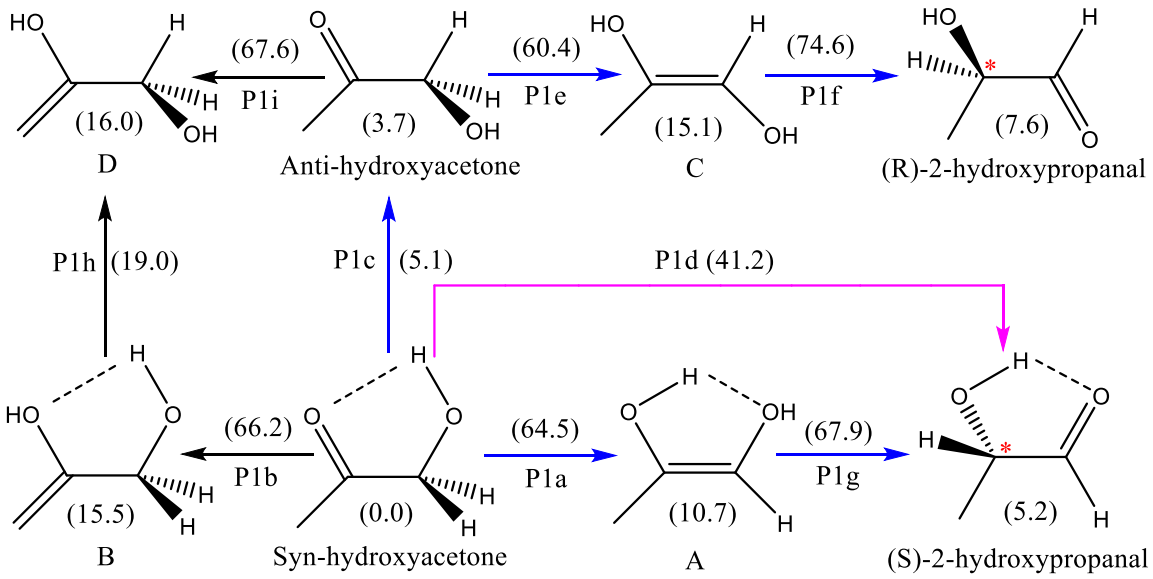

Scheme 1. Possible isomerization pathways of hydroxyacetone (numbers in parentheses are single point energies and energy barriers relative to syn-hydroxyacetone in kcal/mol, with ZPE corrections).

group via P1a to give an enol type isomer A, while the H in -CH_3 migrates to the carbonyl group via P1b to give another enol-type isomer B. The H in -OH can move directly to the carbonyl group via P1d to form (S)-2-hydroxypropanal because of the effect of intramolecular H-bond. Among these three H-migration reactions, P1d is the most energetically favorable pathway with an energy barrier of 41.2 kcal/mol. Anti-hydroxyacetone has two isomerization pathways. H migrations via P1e and Pli produce the enol isomers C and D, respectively. Isomers A and C are enediol intermediates and can further isomerize to (S)-2-hydroxypropanal and (R)-2-hydroxypropanal via P1f and P1g by migration of the H on -OH, respectively. Isomerization to P1f has the highest energy barrier with respect to syn-hydroxyacetone (74.6 kcal/mol) among all the isomerization pathways. The structures of the species presented in Scheme 1 are closely related. Syn-

hydroxyacetone and anti-hydroxyacetone are conformers, and so are B and D. A and C are cis-trans isomers. (S)-2-hydroxypropanal and (R)-2-hydroxypropanal are optical isomers.

3.2.2 Thermal Decomposition of Hydroxyacetone

The bond dissociation energy (BDE) values of syn- and anti-hydroxyacetone were calculated and provided in Table S2 in SI. The bond homolysis between the carbonyl carbon and the carbon attached to the hydroxyl group (C_{CO}-C_{COH}) via P2a, producing the CH_3CO + CH_2OH radicals, is found to be the most energetically favored pathway with an energy threshold of 72.4 kcal/mol in Fig. 4. The BDE values of bond homolysis reaction R3 and R6 are higher than that of P2a. R3 gives CH_3 and $OCCH_2OH$ (m/z 59) radicals. Bond homolysis R4 has the highest energy threshold

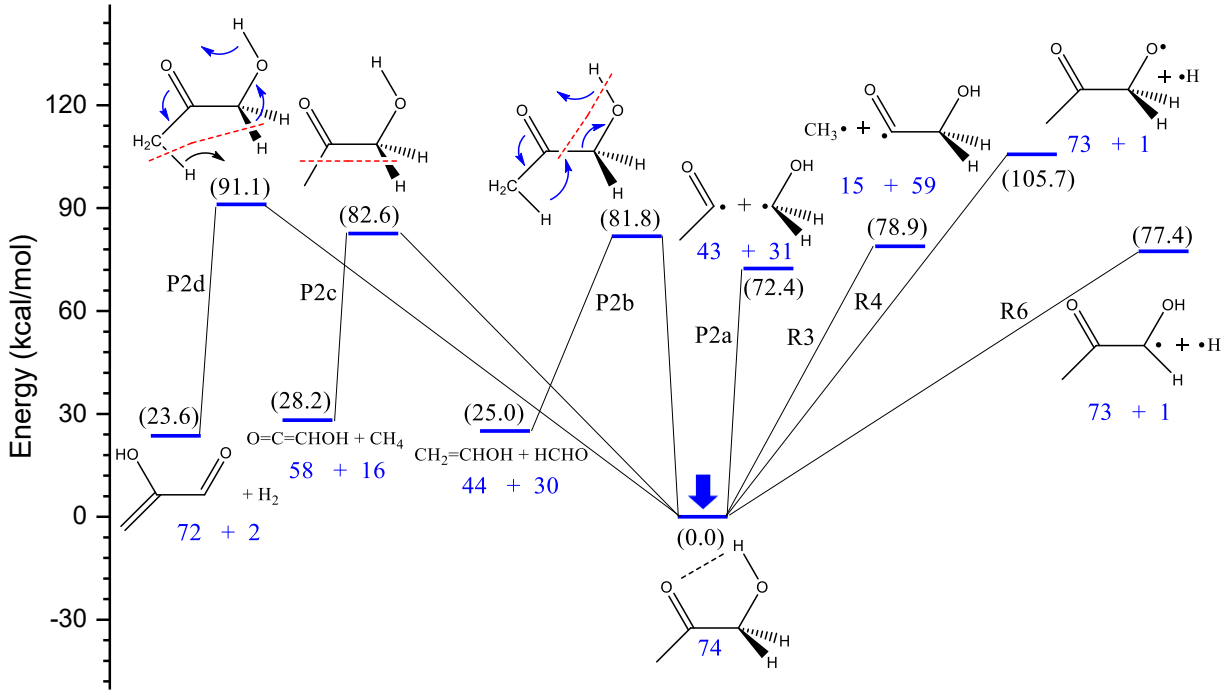

Fig. 4 Possible decomposition pathways of syn-hydroxyacetone. Numbers in parentheses are single point energies and energy barriers relative to syn-hydroxyacetone in kcal/mol, with ZPE corrections. Numbers in blue are m/z values.

of 105.7 kcal/mol, thus least likely to occur. Three molecular elimination pathways (P2b, P2c, and P2d) of syn-hydroxyacetone are determined. Formaldehyde elimination of syn-hydroxyacetone via P2b yields ethenol (m/z 44) with an energy barrier of 81.8 kcal/mol. In the process of P2b, the H in the hydroxyl group migrates to the carbonyl group to form a new hydroxyl group. Meanwhile, the H in the methyl group migrates to the carbonyl group and forms a new bond with the carbonyl carbon. The elimination of methane from syn-hydroxyacetone via P2c has a slightly higher energy barrier with a value of 82.6 kcal/mol. The by-product of methane via P2c is hydroxyl ketene, and this may explain the small increase in m/z 58 in Fig. 2. The H_2 elimination of syn-hydroxyacetone via P2d occurs at 91.1 kcal/mol, which is much higher than that of P2b and P2c. The H atoms eliminated are from the methyl and methylene groups, respectively.

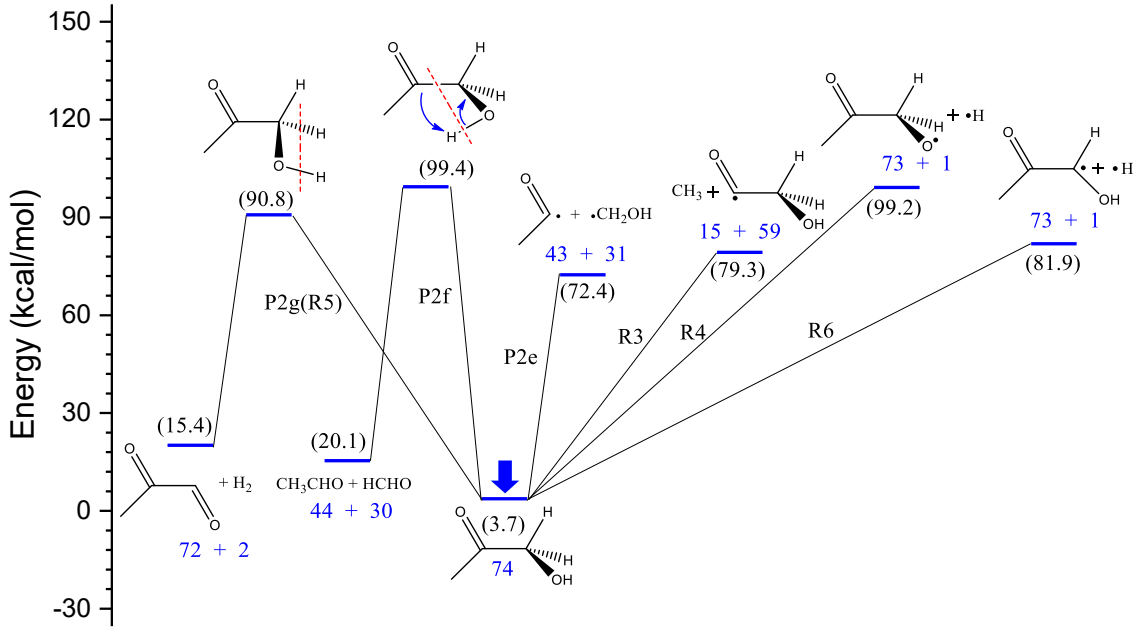

Fig. 5 Possible decomposition pathways of anti-hydroxyacetone. Numbers in parentheses are single point energies and energy barriers relative to syn-hydroxyacetone in kcal/mol, with ZPE corrections. Numbers in blue are m/z values.

The possible unimolecular decomposition pathways of anti-hydroxyacetone are shown in Fig. 5. The pathway P2e to the CH_3CO + CH_2OH products, corresponding to the homolysis of the C_{CO}-C_{COH} bond, has a relatively low bond dissociation energy of 72.4 kcal/mol with respect to syn-hydroxyacetone, showing that P2e is the most energetically favorable decomposition pathway. The BDEs of other homolysis pathways, such as R3, R4 and R6, are similar to those in syn-hydroxyacetone. Formaldehyde elimination of anti-hydroxyacetone via P2f is unlikely to occur due to its high energy barrier (99.4 kcal/mol) with respect to syn-hydroxyacetone. The energy barrier of H_2 elimination of anti-hydroxyacetone via P2g is 90.8 kcal/mol with respect to syn-hydroxyacetone, which is similar to P2d for syn-hydroxyacetone. It should be noted that the co-products of the formaldehyde and H_2 elimination of anti-hydroxyacetone are different from those of syn-hydroxyacetone because of the different initial configurations.

The VTST/TST calculations were performed for decomposition of both syn-hydroxyacetone and anti-hydroxyacetone in order to reveal the competition among the homolysis and molecular elimination pathways. Fig. 6 shows the reaction rate constant curves from 700-1400 K of the pathways with energy barriers lower than 85.0 kcal/mol (those with energy barriers greater than 85.0 kcal/mol are considered as less competitive). Homolysis pathways P2a, P2e, and R3 have large reaction rate constants compared with homolysis R6 and molecular elimination pathways (P2b and P2c). The homolysis products of the C_{CO}-C_{COH} bond of hydroxyacetone via P2a and P2e are the CH_3CO and CH_2OH radicals, which can further decompose by loss of H atom or methyl radical. The decomposition of CH_3CO radical yields CO and methyl radical with an energy barrier of 12.2 kcal/mol with respect to CH_3CO radical, and produces ketene and H atom with an energy

barrier of 42.3 kcal/mol. This indicates that methyl radical is energetically more favorable to be produced than ketene. The H loss of the CH_2OH radical produces formaldehyde. R3 relates to the formation of CH_3 and $OCCH_2OH$ (m/z 59) radicals; R3 (syn-hydroxyacetone) becomes important at the highest temperatures. $OCCH_2OH$ (m/z 59) can further lose an H atom to form OC=CHOH(m/z=58); this may be another source of the m/z 58 peak.

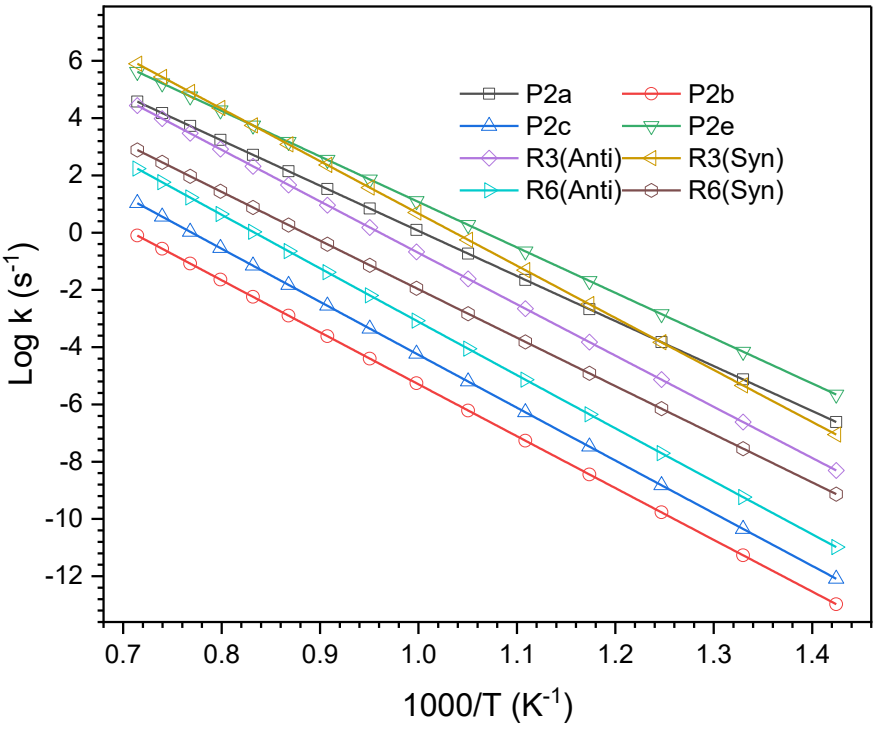

Fig. 6 Reaction rate constants of possible decomposition pathways of hydroxyacetone from 700-1400 K.

3.2.3 Thermal Decomposition of 2-Hydroxypropanal

The BDEs of (S)- and (R)-2-hydroxypropanal were calculated and provided in Table S3 in SI. The three lowest energy homolysis pathways are shown in Fig. 7. The homolysis of the C_{CO}-C_{COH} bond of (S)-2-hydroxypropanal via P3a forms the $CH_3C(H)OH$ and HCO radicals. The dissociation energy of the C_{CO}-C_{COH} bond is 76.0 kcal/mol with respect to syn-hydroxyacetone.

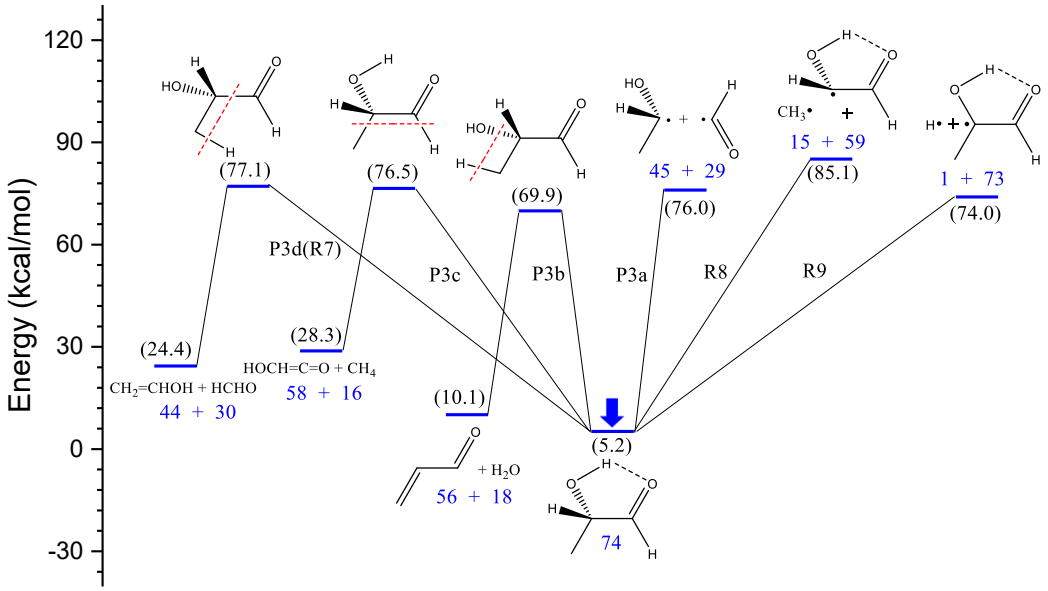

Fig. 7 Possible decomposition pathways of (S)-2-hydroxypropanal. Numbers in parentheses are single point energies and energy barriers relative to syn-hydroxyacetone in kcal/mol, with ZPE corrections. Numbers in blue are m/z values.

The H loss pathway via R9 has an energy threshold of 74.0 kcal/mol. R8 has the highest dissociation energy among all the pathways including molecular elimination channels, indicating that R8 is energetically unfavorable. The H_2O elimination of (S)-2-hydroxypropanal via P3b has the lowest energy barrier (69.9 kcal/mol) with respect to syn-hydroxyacetone. (S)-2-hydroxypropanal can decompose via two additional molecular elimination pathways. The methane elimination of (S)-2-hydroxypropanal through P3c is similar to that of P2c. P3c needs to overcome an energy barrier of 76.5 kcal/mol to form hydroxyl ketene and methane. The formaldehyde elimination of (S)-2-hydroxypropanal via P3d (R7) also has a similar energy barrier (77.1 kcal/mol) with respect to syn-hydroxyacetone.

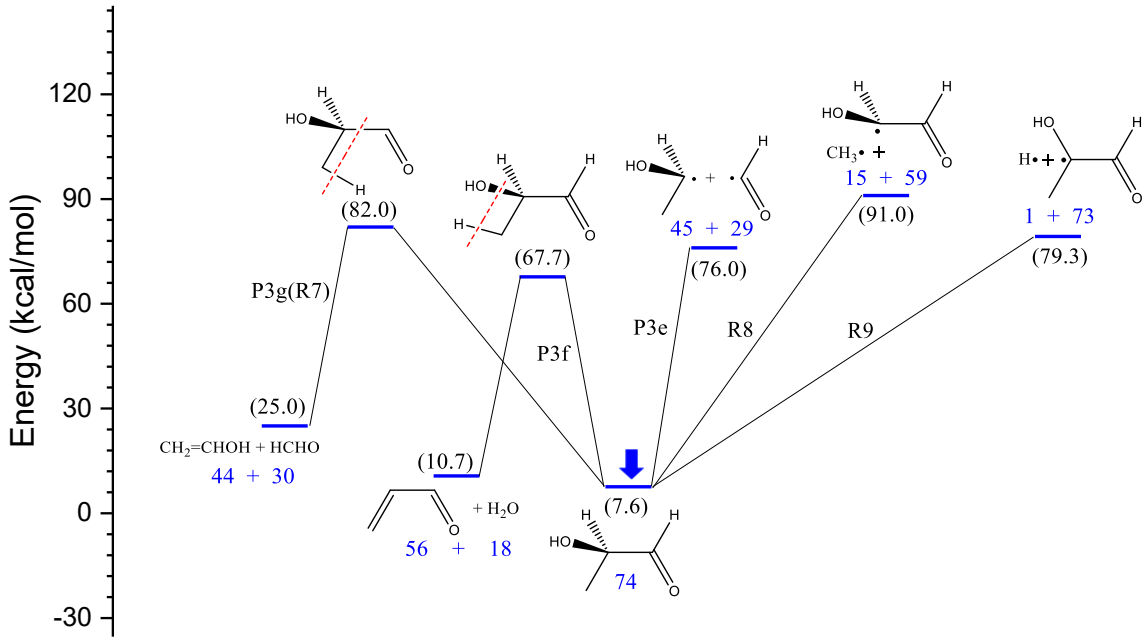

Fig. 8 Possible decomposition pathways of (R)-2-hydroxypropanal. P3e-3g: numbers in parentheses are single point energies and energy barriers relative to syn-hydroxyacetone in kcal/mol, with ZPE corrections. Number in blue are m/z values.

The possible decomposition pathways of (R)-2-hydroxypropanal are shown in Fig. 8. The homolysis of the C_{CO}-C_{COH} bond of (R)-2-hydroxypropanal via P3e forms the $CH_3C(H)OH$ and HCO radicals. The dissociation energy of the C_{CO}-C_{COH} bond is 76.0 kcal/mol with respect to syn-hydroxyacetone. The H-loss R8 and CH_3-loss R9 of (R)-2-hydroxypropanal have larger energy barriers than those in (S)-2-hydroxypropanal. Direct H_2O elimination of (R)-2-hydroxypropanal takes place via P3f, leading to 2-propenal with a relatively low energy barrier of 67.7 kcal/mol with respect to syn-hydroxyacetone. The formaldehyde elimination of (R)-2-hydroxypropanal via P3g produces ethenol as a co-product. The elimination mechanism of P3g (R7) is simpler compared with P2b, involving elimination of the carbonyl group and the adjacent H in methyl group.

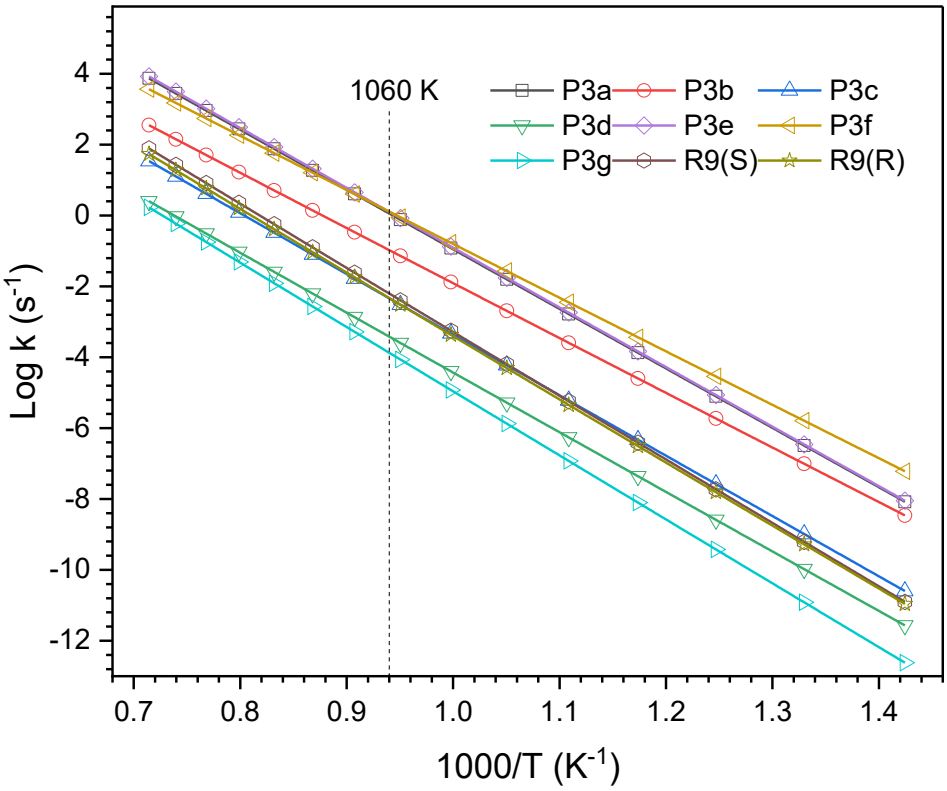

Fig. 9 Reaction rate constants of possible decomposition pathways of 2-hydroxypropanal from 700-1400 K.

The homolytic and molecular elimination decomposition pathways of (S)- and (R)-2-hydroxypropanal have similar energy barrier or threshold. In order to determine the main pathway amongst these, the VTST/TST calculations were performed for their decomposition pathways with energy threshold or barrier below 85 kcal/mol. As shown in Fig. 9, the overall trend of the rate constant k is consistent with the values of the energy barriers. Noteworthily, the rate constant of homolysis of the C_{CO}-C_{COH} bond of (S)-2-hydroxypropanal via P3a (black line, which mostly overlapped with that of C_{CO}-C_{COH} bond homolysis P3e, purple line) is larger than that of H_2O elimination P3b (red line) even though P3b has a relatively lower energy barrier. This is consistent

with the fact that the H_2O molecular elimination P3b proceeds via a reaction barrier and a tight transition state (with a smaller preexponential factor), while the C_{CO}-C_{COH} bond homolysis P3a proceeds via a loose transition state (with a larger preexponential factor), which could make P3a more competitive than P3b in the initial thermal decomposition of hydroxyacetone at the modest temperatures, even though the former has a slightly higher activation energy. This shows that the homolysis of the C_{CO}-C_{COH} bond via P3a is the main initial decomposition reaction. This conclusion is also supported by the experimental results that the first distinguishable peak at m/z 45 corresponding to the $CH_3C(H)OH$ radical was found at 950 K, while only a small peak at m/z 56 corresponding to 2-propenal in the H_2O elimination pathway P3b was found at 1230 K. At higher temperatures, the H_2O molecular elimination became more significant as observed. For (R)-2-hydroxypropanal, the C_{CO}-C_{COH} bond homolysis P3e and H_2O elimination P3f have larger rate constants than other pathways in (R)-2-hydroxypropanal. The rate constant of P3e becomes greater than that of P3f over 1060 K. This indicates that the homolysis of the C_{CO}-C_{COH} bond via P3e and the water elimination pathway P3f are the main initial decomposition pathway of (R)-2-hydroxypropanal. R9 and P3c have medium rate constant k, and R7 (P3d or P3g) have the smallest rate constant k. These pathways are less competitive than the C_{CO}-C_{COH} bond homolysis pathways (P3a and P3e) and the H_2O elimination pathways (P3b and P3f).

4. Discussions

4.1 Initiation Reactions

Based on the energetics calculation results, the energy barriers of isomerization reactions of hydroxyacetone (41.2-74.6 kcal/mol) are significantly lower than those of the unimolecular decomposition reactions of hydroxyacetone (67.7-105.7 kcal/mol). This implies that the isomerization reactions can take place prior to and in competition with the thermal decomposition reactions. Therefore, the conformers and isomers of hydroxyacetone contribute to the initial thermal decomposition reactions and their intermediates and products. However, the initial decomposition pathways of isomers labeled as A, B, C and D in the enol form are much less important and are not further considered. The reason is that it is relatively more difficult to break the C-C double bond compared to the C-C σ single bond. In addition, the planar structure of enol-type isomers hinders concerted molecular elimination due to the steric effect. The H_2O elimination pathways of the enol-type isomers were examined theoretically here. These pathways obviously have greater energy barriers (87-95 kcal/mol, seen Table S4 in SI) than that of P3b and P3f (69.9 and 67.7 kcal/mol).

As shown in Fig. 1, the CH_3CO (m/z 43), $CH_3C(H)OH$ (m/z 45) and CH_3 (m/z 15) radicals were found at medium temperatures (950-1140 K). It demonstrates that the homolysis reactions dominate the initial thermal decomposition reactions of hydroxyacetone. The CH_3CO radical at m/z 43 is produced by the homolysis of the C_{CO}-C_{COH} bond of hydroxyacetone via P2a and P2e The $CH_3C(H)OH$ radical (m/z 45) is formed by the homolysis of the C_{CO}-C_{COH} bond of 2-hydroxypropanal via P3a and P3e. The calculated reaction energetics and rate constants also

support that the pathways corresponding to the C_{CO}-C_{COH} bond dissociation are the main initial pathways. The CH_3-loss R3 and H-loss R6 have higher energy barriers (77.4-81.9 kcal/mol), and the kinetic calculations show that the rate constants of R3 are obviously greater than those of R6. Especially for R3 of syn-hydroxyacetone, the corresponding rate constant becomes the greatest among all the R3 and R6 decomposition pathways, and at the highest temperature, it becomes competitive with that of P2a and P2e. The m/z 15 and 59 peaks would be generated when R3 occurred. While m/z 15 was prominent at high temperature, m/z 59 was of small intensity in the mass spectra. One possible reason is that the m/z 59 radical underwent secondary loss of an H atom to form OC=CHOH(m/z=58), which was found to increase at > 1230 K in the mass spectra. Therefore, R3 is a possible initial decomposition pathway. The m/z 73 peak was observed with very small or nearly no intensity at and above 1230 K, indicating very small contributions from the R6 pathways. H-loss R4 and CH_3-loss R8 are not considered as the initial decomposition pathways since their BDE values are greater than 85 kcal/mol.

Small molecules, such as H_2, methane, H_2O, and formaldehyde can be produced by direct molecular eliminations of hydroxyacetone and 2-hydroxypropanal. The corresponding peaks of the co-products are at m/z 72, 58, 56, and 44. However, these peaks produced by the initial thermal decomposition were not detected in the initial temperature range of 950-1140 K but only at higher temperature range above 1190 K, showing that the concerted molecular elimination reactions are not important as the initial pathways at the medium temperatures of 950-1140 K. The energy barriers of the H_2, CH_4, and HCHO molecular eliminations of hydroxyacetone are greater than 81.8 kcal/mol, which is higher than that of the homolysis of the C_{CO}-C_{COH} bond (72.4 kcal/mol in

syn- and anti-hydroxyacetone). The energy barriers of the CH_4 and HCHO molecular eliminations of 2-hydroxypropanal are in the range of 76.5-82.0 kcal/mol. These energy comparisons render that the C_{CO}-C_{COH} bond homolysis is more competitive than the H_2, CH_4, and HCHO molecular elimination pathways, consistent with the observed pyrolysis mass spectra of hydroxyacetone (Fig. 1 and 2). The energy barrier of the concerted H_2O elimination of (S)-2-hydroxypropanal via P3b is only 69.9 kcal/mol. However, as indicated by the TST/VTST calculations, the rate constant of the H_2O elimination P3b is lower than those of the C_{CO}-C_{COH} bond homolysis P3a and P3e. This is confirmed by the pyrolysis mass spectra. The CH_3CO (m/z 43) and $CH_3C(H)OH$ (m/z 45) radicals produced by the homolysis pathways were found at 950 K. In comparison, the m/z 56 peak (co-product of H_2O elimination) appeared at ~ 1230 K, indicating that P3b occurred at higher temperatures than the C_{CO}-C_{COH} bond homolysis of hydroxyacetone. At higher temperatures, the H_2O molecular elimination became more significant. The energy barrier of the H_2O molecular elimination of (R)-2-hydroxypropanal via P3f is only 67.7 kcal/mol. The TST/VTST rate constant calculations showed that the P3f pathway was more important than the C_{CO}-C_{COH} bond homolysis P3a and P3e at temperatures below 1060 K. This is not consistent with the pyrolysis mass spectra. It is not clear what causes the discrepancy, and further improvements of the energetic and kinetic calculations could be needed. One possible reason is that there are four steps from syn-hydroxyacetone to the H_2O elimination of (R)-2-hydroxypropanal (P1c→P1e→P1f→P3f) according to Scheme 1 and Fig. 8. The isomerization reaction P1f is the rate-determining step with the greatest energy barrier of 74.6 kcal/mol. Therefore, the m/z 56 peak from the H_2O elimination was not shown in the mass spectra at the initial and medium temperatures even though P3f has a

relatively large rate constant.

4.2 Secondary Decomposition Reactions

Secondary decomposition reactions mainly refer to the subsequent decomposition reactions of the radical intermediates produced from the initial decomposition reactions in this study. These radical intermediates can be further activated by secondary thermal collisions with the buffer gas (which is > 99% of the gas mixture) at more elevated temperatures above the initiation temperature. The CH_3CO radical (m/z=43), produced by the cleavage of the C_{CO}-C_{COH} bond via P2a and P2e, decomposes by loss of a methyl radical (m/z 15) with an energy threshold of 12.2 kcal/mol (by the DFT calculation). The CH_3CO radical can also lose a hydrogen atom on the methyl group to form ketene (m/z 42) with an energy threshold of 42.3 kcal/mol. Fig. 3 clearly shows that the intensities of the peaks of ketene and methyl radical gradually increased with the decrease of the intensity of CH_3CO radical starting from 1190 K. This experimental result confirms the subsequent decomposition pathways of CH_3CO radical proposed based on the DFT calculations. The CH_2OH radical (m/z 31), the counterpart of CH_3CO radical in the homolysis of C_{CO}-C_{COH} bond of hydroxyacetone, decomposes by losing one H atom to form formaldehyde (m/z 30) with an energy barrier of 35.9 kcal/mol. This is consistent with the increase of m/z 31 peak to its maximum from 1140 K to 1270 K, followed by a slight decrease in intensity from 1310 K to 1390 K (Fig. 1 and 2). The peak of formaldehyde was not observed throughout the whole temperature range because of its high ionization energy (IP=10.86 eV).[46]

The cleavage of the C_{CO}-C_{COH} bond of 2-hydroxypropanal via P3a and P3e generates the

$CH_3C(H)OH$ and HCO radicals. The $CH_3C(H)OH$ radical (m/z 45) can eliminate the H atom in the methyl group to form ethenol (m/z 44) with an energy threshold of 25.9 kcal/mol or the H atom in the hydroxyl group to form acetaldehyde (m/z 44) with an energy threshold of 38.1 kcal/mol, respectively. The ethenol + H pathway is more favorable due to its lower energy. From the pyrolysis mass spectra, the first distinguishable peak of ethenol or acetaldehyde at m/z 44 was found at 1230 K, while the peak of $CH_3C(H)OH$ radical at m/z 45 was found at 950 K. This indicates that $CH_3C(H)OH$ radical is formed prior to ethenol or acetaldehyde. The intensity evolution curves in Fig. 3 also show that the intensity of the m/z 44 peak increased accordingly and significantly with the decrease in intensity of the m/z 45 peak when the temperature was above 1230 K. In other words, the amounts of ethenol or acetaldehyde increase with the depletion of the $CH_3C(H)OH$ radical. It should be pointed out that ethenol (m/z 44) can also be generated by formaldehyde elimination via P2b and P3d (R7). However, pathways P2b and P3d are much less important as their energy barriers are greater than that for the homolytic production of the $CH_3C(H)OH$ radical (which can then undergo the H loss upon activation by secondary collisions). The HCO radical (m/z 29), the co-product of the $CH_3C(H)OH$ radical formed via P3a and P3e, decomposes into H atom and CO (m/z 28). The peak of the HCO radical was clearly observed at 1270 K, while the peak of CO was not found in the pyrolysis spectra due to its high ionization energy (14.00 eV).[47]

4.3 α-H Reactivity and Elimination Reactions

In addition to the homolysis reactions in the process of hydroxyacetone pyrolysis, reactions

involving α-H are also important. It is well known that the α-H of aldehyde or ketone is acidic because of the inductive effect of the carbonyl group. The activity of α-H enables the keto-enol tautomerisms. Hydroxyacetone has two types of α-H, the H atom in $-CH_3$ group and the H atom in $-CH_2-$ group. The reactivity of the α-H in the $-CH_2-$ group is higher than that in the $-CH_3$ group because the OH group attached to the $-CH_2-$ group enhances the inductive effect. This conclusion is evident from the calculation results that the energy barrier of P1b involving the α-H in CH_3 is greater than that of P1a involving the α-H in $-CH_2-$ group. A similar result can be obtained by comparing the pathways of P1e and P1i. Another type of reactions related to α-H are H_2 elimination reactions. H_2 can be formed by P2d and P2g (R5) involving the α-H in the $-CH_2-$ group of hydroxyacetone. The peak of the co-product of H_2 at m/z 72 was found above 1190 K. The energy barriers of P2d and P2g (R5) are 81.8 and 90.8 kcal/mol with respect to syn-hydroxyacetone. The energy barrier values suggest that P2d is more energetically favorable than R5.

CH_4, formaldehyde and H_2O elimination reactions are also related to α-H, and are not negligible at high temperatures (> 1190 K) except for the H_2 elimination reactions. CH_4 can be produced via P2c and P3c. The appearance of the peak of the CH_4 co-product at m/z 58 manifests that P2c and P3c are present in the process of hydroxyacetone pyrolysis. P2b, P2f, P3d (R7) and P3g (R7) are four different pathways of formaldehyde formation by direct molecular elimination. The peak of the co-product of formaldehyde at m/z 44 was found at temperatures above 1230 K. Among these pathways, P3d (R7) has the lowest energy barrier with a value of 77.1 kcal/mol with respect to syn-hydroxyacetone. The direct formation of H_2O during the pyrolysis of hydroxyacetone has not been reported in the literature. The formation pathways of H_2O via P3b and P3f are verified in the

present study. The peak of the co-product of H_2O at m/z 56 was also observed when the temperature was greater than 1230 K.

5. Conclusions

The thermal decomposition mechanism of hydroxyacetone has been studied systemically by using VUV-PI-TOFMS combined with the DFT calculations. The results show that the keto-enol tautomerism can occur when the temperature is not high enough to cause thermal decomposition. Possible decomposition pathways of syn-hydroxyacetone, anti-hydroxyacetone, (S)-2-hydroxypropanal and (R)-2-hydroxypropanal are discussed in the present work. Thermal decomposition reactions occurred from about 950 K. Homolysis reactions involving the C_{CO}-C_{COH} bond via P2a, P2e, P3a and P3e, as well as the homolytic CH_3-loss R3, are determined as the main initial decomposition reactions. The subsequent decompositions of the radical intermediates ($\cdot CH_3CO$, $\cdot CH_2OH$, $\cdot CH_3C(H)OH$ and $\cdot HCO$) are considered as the main secondary decomposition reactions. Elimination reactions to produce small molecules, such as H_2O, H_2, CH_4 and HCHO, were identified at temperatures above 1230 K, with the H_2O elimination being the most important molecular elimination channels. The active α-H atoms play an important role in these elimination reactions. The detailed mechanism of the thermal decomposition of hydroxyacetone would provide useful insights for improving steam reforming and thermal conversion of biomass and bio-oil.

Acknowledgement

This work was supported by the US National Science Foundation (NSF CHE-2155232). KLS acknowledges support from a UC President's Dissertation-Year Fellowship. XHL acknowledges the support from the program of China Scholarships Council (No. 201606440042).

Declaration of Conflicting Interests Statement

The Authors declare no competing financial interest.

Supporting Information

Relative energies of isomers with respect to syn-hydroxyacetone calculated at different level of theories, the BDE values of hydroxyacetone and 2-hydroxypropanal, the energy barriers of H_2O elimination pathways of the enol isomers, and the calculated Cartesian coordinates of the species involved in the hydroxyacetone and 2-hydroxypropanal thermal decompositions.

References

(1) de Souza, R. O. M. A.; Miranda, L. S. M.; Luque, R., Bio(chemo)technological strategies for biomass conversion into bioethanol and key carboxylic acids. *Green Chemistry* **2014**, *16*, 2386-2405.

(2) Zhang, X., Essential scientific mapping of the value chain of thermochemically converted

second-generation bio-fuels. *Green Chemistry* **2016**, *18*, 5086-5117.

(3) Trane, R.; Dahl, S.; Skjøth-Rasmussen, M. S.; Jensen, A. D., Catalytic steam reforming of bio-oil. *International Journal of Hydrogen Energy* **2012**, *37*, 6447-6472.

(4) Dubey, V. R.; Vaidya, P. D., Kinetics of steam reforming of acetol over a Pt/C catalyst. *Chemical Engineering Journal* **2012**, *180*, 263-269.

(5) Gutiérrez Ortiz, F. J.; Campanario, F. J.; Ollero, P., Supercritical water reforming of model compounds of bio-oil aqueous phase: Acetic acid, acetol, butanol and glucose. *Chemical Engineering Journal* **2016**, *298*, 243-258.

(6) Fuentes-Cano, D.; Gómez-Barea, A.; Nilsson, S.; Ollero, P., Kinetic Modeling of Tar and Light Hydrocarbons during the Thermal Conversion of Biomass. *Energy & Fuels* **2016**, *30*, 377-385.

(7) Zheng, M.; Wang, Z.; Li, X.; Qiao, X.; Song, W.; Guo, L., Initial reaction mechanisms of cellulose pyrolysis revealed by ReaxFF molecular dynamics. *Fuel* **2016**, *177*, 130-141.

(8) Uemura, K.; Appari, S.; Kudo, S.; Hayashi, J.-i.; Einaga, H.; Norinaga, K., In-situ reforming of the volatiles from fast pyrolysis of ligno-cellulosic biomass over zeolite catalysts for aromatic compound production. *Fuel Processing Technology* **2015**, *136*, 73-78.

(9) Norinaga, K.; Yang, H.; Tanaka, R.; Appari, S.; Iwanaga, K.; Takashima, Y.; Kudo, S.; Shoji, T.; Hayashi, J.-i., A mechanistic study on the reaction pathways leading to benzene and naphthalene in cellulose vapor phase cracking. *Biomass and Bioenergy* **2014**, *69*, 144-154.

(10) Huang, J.; He, C.; Wu, L.; Tong, H., Theoretical studies on thermal decomposition mechanism of arabinofuranose. *Journal of the Energy Institute* **2017**, *90*, 372-381.

(11) Ryozo, G.; Jun'ichi, H.; Kenichi, K.; Sinichi, O., Studies on the Chemical Decomposition of

Simple Sugars. X. Acetol Formation from 14C-Labeled Hexoses. *Bulletin of the Chemical Society of Japan* **1961**, *34*, 753-757.

(12) Hu, B.; Lu, Q.; Jiang, X.-y.; Liu, J.; Cui, M.-s.; Dong, C.-q.; Yang, Y.-p., Formation mechanism of hydroxyacetone in glucose pyrolysis: A combined experimental and theoretical study. *Proceedings of the Combustion Institute* **2019**, *37*, 2741-2748.

(13) Velasquez, M.; Santamaria, A.; Batiot-Dupeyrat, C., Selective conversion of glycerol to hydroxyacetone in gas phase over La2CuO4 catalyst. *Applied Catalysis B: Environmental* **2014**, *160-161*, 606-613.

(14) Papageridis, K. N.; Siakavelas, G.; Charisiou, N. D.; Avraam, D. G.; Tzounis, L.; Kousi, K.; Goula, M. A., Comparative study of Ni, Co, Cu supported on γ-alumina catalysts for hydrogen production via the glycerol steam reforming reaction. *Fuel Processing Technology* **2016**, *152*, 156-175.

(15) Lari, G. M.; Pastore, G.; Haus, M.; Ding, Y.; Papadokonstantakis, S.; Mondelli, C.; Perez-Ramirez, J., Environmental and economical perspectives of a glycerol biorefinery. *Energy & Environmental Science* **2018**, *11*, 1012-1029.

(16) Chuang-Wei, C.; Ali, T.; R., S. W.; M., R. J.; J., S. G., Low-pressure packed-bed gas phase conversion of glycerol to acetol. *AIChE Journal* **2008**, *54*, 2456-2463.

(17) Bimbela, F.; Oliva, M.; Ruiz, J.; García, L.; Arauzo, J., Catalytic steam reforming of model compounds of biomass pyrolysis liquids in fixed bed: Acetol and n-butanol. *Journal of Analytical and Applied Pyrolysis* **2009**, *85*, 204-213.

(18) Chen, D.; Cen, K.; Chen, F.; Ma, Z.; Zhou, J.; Li, M., Are the typical organic components in

biomass pyrolyzed bio-oil available for leaching of alkali and alkaline earth metallic species (AAEMs) from biomass? *Fuel* **2020**, *260*, 116347.

(19) Ramos, M. C.; Navascués, A. I.; García, L.; Bilbao, R., Hydrogen Production by Catalytic Steam Reforming of Acetol, a Model Compound of Bio-Oil. *Industrial & Engineering Chemistry Research* **2007**, *46*, 2399-2406.

(20) Wang, S.; Cai, Q.; Zhang, F.; Li, X.; Zhang, L.; Luo, Z., Hydrogen production via catalytic reforming of the bio-oil model compounds: Acetic acid, phenol and hydroxyacetone. *International Journal of Hydrogen Energy* **2014**, *39*, 18675-18687.

(21) Albuquerque, E. M.; Borges, L. E. P.; Fraga, M. A., Lactic acid production from hydroxyacetone on dual metal/base heterogeneous catalytic systems. *Green Chemistry* **2015**, *17*, 3889-3899.

(22) Jing, S.; Sui, S.; Gabriel, d. S., The gas phase aldose-ketone isomerization mechanism: Direct interconversion of the model hydroxycarbonyls 2-hydroxypropanal and hydroxyacetone. *International Journal of Quantum Chemistry* **2017**, *117*, e25434.

(23) de Araújo, M. L.; Mandelli, D.; Kozlov, Y. N.; Carvalho, W. A.; Shul'pin, G. B., Oxidation of hydroxyacetone (acetol) with hydrogen peroxide in acetonitrile solution catalyzed by iron(III) chloride. *Journal of Molecular Catalysis A: Chemical* **2016**, *422*, 103-114.

(24) Chambreau, S. D.; Zhang, J.; Traeger, J. C.; Morton, T. H., Photoionization of methyl t-butyl ether (MTBE) and t-octyl methyl ether (TOME) and analysis of their pyrolyses by supersonic jet/photoionization mass spectrometry. *International Journal of Mass Spectrometry* **2000**, *199*, 17-27.

(25) Chambreau, S. D.; Zhang, J., VUV photoionization time-of-flight mass spectrometry of flash pyrolysis of silane and disilane. *Chemical Physics Letters* **2001**, *343*, 482-488.

(26) Lemieux, J. M.; Zhang, J., Thermal decomposition of tetramethylsilane and tetramethylgermane by flash pyrolysis vacuum ultraviolet photoionization time-of-flight mass spectrometry. *International Journal of Mass Spectrometry* **2014**, *373*, 50-55.

(27) Jones, P. J.; Riser, B.; Zhang, J., Flash Pyrolysis of t-Butyl Hydroperoxide and Di-t-butyl Peroxide: Evidence of Roaming in the Decomposition of Organic Hydroperoxides. *The Journal of Physical Chemistry A* **2017**, *121*, 7846-7853.

(28) Liu, X.; Zhang, J.; Vazquez, A.; Wang, D.; Li, S., Mechanism of the thermal decomposition of tetramethylsilane: a flash pyrolysis vacuum ultraviolet photoionization time-of-flight mass spectrometry and density functional theory study. *Physical Chemistry Chemical Physics* **2018**, *20*, 18782-18789.

(29) Petitjean, M.; Reyès-Pérez, E.; Pérez, D.; Mirabel, P.; Le Calvé, S., Vapor Pressure Measurements of Hydroxyacetaldehyde and Hydroxyacetone in the Temperature Range (273 to 356) K. *Journal of Chemical & Engineering Data* **2010**, *55*, 852-855.

(30) Kohn, D. W.; Clauberg, H.; Chen, P., Flash pyrolysis nozzle for generation of radicals in a supersonic jet expansion. *Review of Scientific Instruments* **1992**, *63*, 4003-4005.

(31) Zhang, X.; Friderichsen, A. V.; Nandi, S.; Ellison, G. B.; David, D. E.; McKinnon, J. T.; Lindeman, T. G.; Dayton, D. C.; Nimlos, M. R., Intense, hyperthermal source of organic radicals for matrix-isolation spectroscopy. *Review of scientific instruments* **2003**, *74*, 3077-3086.

(32) Guan, Q.; Urness, K. N.; Ormond, T. K.; David, D. E.; Barney Ellison, G.; Daily, J. W., The

properties of a micro-reactor for the study of the unimolecular decomposition of large molecules. *International Reviews in Physical Chemistry* **2014**, *33*, 447-487.

(33) Weddle, P. J.; Karakaya, C.; Zhu, H.; Sivaramakrishnan, R.; Prozument, K.; Kee, R. J., Boundary-Layer Model to Predict Chemically Reacting Flow within Heated, High-Speed, Microtubular Reactors. *International Journal of Chemical Kinetics* **2018**, *50*, 473-480.

(34) Liu, C.; Ye, L.; Yuan, W.; Zhang, Y.; Zou, J.; Yang, J.; Wang, Y.; Qi, F.; Zhou, Z., Investigation on pyrolysis mechanism of guaiacol as lignin model compound at atmospheric pressure. *Fuel* **2018**, *232*, 632-638.

(35) Fukui, K., The path of chemical reactions - the IRC approach. *Accounts of Chemical Research* **1981**, *14*, 363-368.

(36) Frisch, M. J.; Trucks, G. W.; Schlegel, H. B.; Scuseria, G. E.; Robb, M. A.; Cheeseman, J. R.; Scalmani, G.; Barone, V.; Mennucci, B.; Petersson, G. A., et al. Gaussian 09, Revision B.01; Gaussian, Inc.: Wallingford, CT, **2010**.

(37) Truhlar, D. G.; Garrett, B. C.; Klippenstein, S. J., Current Status of Transition-State Theory. *The Journal of Physical Chemistry* **1996**, *100*, 12771-12800.

(38) Wigner, E., The transition state method. *Transactions of the Faraday Society* **1938**, *34*, 29-41.

(39) Jasper, A. W.; Miller, J. A.; Klippenstein, S. J., Collision Efficiency of Water in the Unimolecular Reaction CH4 (+H_2O) ⇆ CH_3 + H (+H_2O): One-Dimensional and Two-Dimensional Solutions of the Low-Pressure-Limit Master Equation. *The Journal of Physical Chemistry A* **2013**, *117*, 12243-12255.

(40) Canneaux, S.; Bohr, F.; Henon, E., KiSThelP: A program to predict thermodynamic properties

and rate constants from quantum chemistry results†. **2014**, *35*, 82-93.

(41) Ali, M. A., Computational studies on the gas phase reaction of methylenimine (CH_2NH) with water molecules. *Scientific Reports* **2020**, *10*, 10995.

(42) Shao, K.; Brunson, J.; Tian, Y.; Zhang, J., Flash pyrolysis mechanism of trimethylchlorosilane. *International Journal of Mass Spectrometry* **2022**, *482*, 116933.

(43) Shao, K.; Liu, X.; Zhang, J., Thermal Decomposition Mechanism of Tetraethylsilane by Flash Pyrolysis Vacuum Ultraviolet Photoionization Mass Spectrometry and DFT Calculations: The Competition between β-Hydride Elimination and Bond Homolysis. *The Journal of Physical Chemistry A* **2023**, *127*, 3966-3975.

(44) Mohandas, S.; Ramabhadran, R. O.; Kumar, S. S., Theoretical Investigation of a Vital Step in the Gas-Phase Formation of Interstellar Ammonia $NH_2^+ + H_2 \rightarrow NH_3^+ + H$. *The Journal of Physical Chemistry A* **2020**, *124*, 8373-8382.

(45) Begum, S.; Subramanian, R., Theoretical studies on gas-phase kinetics and mechanism of H-abstraction reaction from methanol by ClO and BrO radicals. *RSC Advances* **2015**, *5*, 39110-39121.

(46) Traeger, J. C., Heat of formation for the formyl cation by photoionization mass spectrometry. *International Journal of Mass Spectrometry and Ion Processes* **1985**, *66*, 271-282.

(47) Rabalais, J. W.; Debies, T. P.; Berkosky, J. L.; Huang, J. T. J.; Ellison, F. O., Calculated photoionization cross sections and relative experimental photoionization intensities for a selection of small molecules. **1974**, *61*, 516-528.

1 TOC Graphic

2

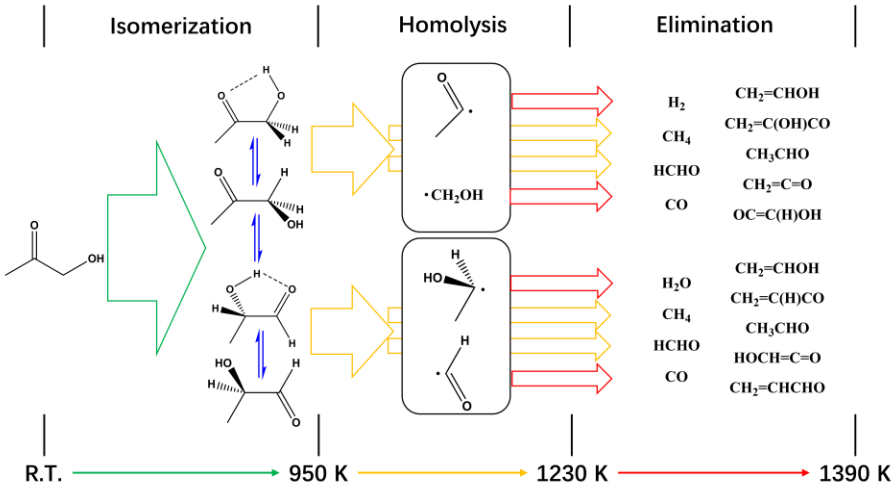

3